A Passive Mixer-First Receiver With Digitally Controlled and Widely Tunable RF Interface

Caroline Andrews, *Student Member, IEEE*, and Alyosha C. Molnar, *Member, IEEE*

***Abstract*—A software-defined radio (SDR) receiver with baseband programmable RF bandpass filter (BPF) and complex impedance match is presented. The passive mixer-first architecture used here allows the impedance characteristics of the receiver's baseband circuits to be translated to the RF port of the receiver. Tuning the resistance at the baseband port allows for a real impedance match to the antenna. The addition of "complex feedback" between I and Q paths allows for matching to the imaginary component of the antenna impedance. By implementing both real and imaginary components with resistors in feedback around low noise baseband amplifiers, noise figure is also kept low. Tunable sampling capacitors on the baseband side of the passive mixer translate to tunable-Q filters on the RF port which allow for very good out-of-band linearity. Furthermore, the concept of in-band and out-of-band must be redefined as the impedance match and BPF center frequency move with the LO frequency, such that matching and filtering track the receive frequency. Additionally, 8-phase mixing is shown to provide significant benefits such as impedance matching range, rejection of blockers at LO harmonics, and lower noise figure (NF). Measurements from the receiver implemented in 65 nm CMOS show 70 dB of gain, NF as low as 3 dB, and 25 dBm out-of-band IIP3. Furthermore, tunable impedance matching shows that $S_{11}<-30$ dB can be achieved at any receive frequency from 0.1–1.3 GHz.**

***Index Terms*—Blocker, blocker filtering, CMOS, harmonic mixing, harmonic rejection, impedance matching, linearity, mixer, multi-phase, multi-phase clock, out-of-band interference, passive mixer, receiver, SAW-less, software-defined radio (SDR), switching receiver, wideband receiver.**

I. Introduction

A software-defined radio (SDR) ideally allows all of the parameters of a radio to be programmed dynamically. In recent years, innovations in both circuit architectures and process technologies have enabled great programmability in bandwidth [1], oscillation frequency [2]–[4], gain, and modulation type. However, the antenna interface of receivers, i.e., the RF LNA, matching network and RF band-pass filter (often a SAW filter), remain very hard to tune [5]–[7].

Ideally, the antenna interface of an RF receiver should perform three functions: 1) match the impedance of the antenna so as to extract the maximum possible wanted (in-band) signal power from the antenna and prevent reflections, 2) amplify the wanted signal with low noise, and 3) reject unwanted (out-of-band) interferers. However, in the current literature, achieving these goals over wide RF tuning range has proven challenging [3], [4]. The structures currently used to achieve both good impedance matching and low susceptibility to blockers require resonant structures that are inherently highly frequency dependent.

Current solutions for receivers capable of capturing several widely spaced bands either involve multiple, parallel, narrowband front-ends, used one at a time [8]–[11], or wideband receivers with only moderate rejection of interference (out-of-band IIP3 of < 0 dBm) at many bands [3], [4], [12]. The former solution comes at significant cost in area both on chip and off, and the latter simply cannot achieve the necessary performance for many applications (cellular, etc.). The current state of the art does not allow for a high performance, high tuning range SDR.

The architecture of high performance (and therefore) narrowband direct conversion receivers includes (in order of the input signal path) an off-chip RF-band filter, a matching network, LNA, mixer, and baseband circuitry [9], [13]. The components which are difficult to tune across frequency are the ones which see the RF signal, coming before the mixer in the signal path. The RF-band filter rejects out-of-band blockers, and is typically implemented with high-Q off-chip components such as SAW filters. The matching network, typically implemented with a resonant *LC* network, transfers as much power as possible to the LNA. The LNA absorbs the RF power and provides amplification of the signal with as little noise as possible. Indeed, a good definition of an LNA is an amplifier that provides an impedance match with less than 3 dB noise figure (something a simple resistive matching network cannot achieve). Widely tunable receivers reported so far remove the RF-band filter entirely and substitute a wideband but lower performance and higher power matched LNA [3], [4].

In principle, a homodyne (direct conversion) receiver does not require any RF components but a mixer and local oscillator in order to function, and indeed early receivers included only these components [14]. This simple approach has recently garnered more attention, as recent work suggests that connecting the antenna directly to a CMOS *passive* mixer without an RF LNA can provide significant benefits, such as extremely low power [15] or greatly increased tuning range and linearity [2], [16]. Interest has been renewed in passive mixers in LNA-first applications as well, because of their high linearity [17]–[19]. The receiver we present here begins with the passive mixer-first approach, eliminating the traditional RF filter, RF matching net-

Manuscript received April 21, 20110; revised July 22, 2010; accepted August 13, 2010. Date of publication October 18, 2010; date of current version December 03, 2010. This paper was approved by Guest Editor Kari Halonen. This work was supported in part by NSF grant no. ECCS-0925670. Chip fabrication was generously provided by the TSMC University Shuttle Program.

The authors are with Cornell University, Ithaca, NY 14853 USA (e-mail: cja67@cornell.edu).

Color versions of one or more of the figures in this paper are available online at http://ieeexplore.ieee.org.

Digital Object Identifier 10.1109/JSSC.2010.2077151

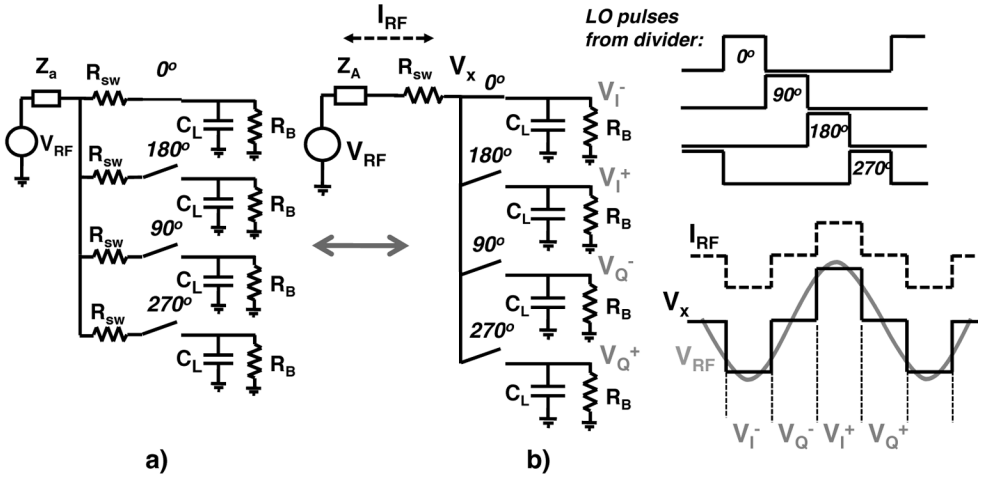

Fig. 1. (a) Model of 4-phase passive mixer with sampling capacitor C_L and load resistor R_B. (b) Equivalent model, with LO driving waveforms and resulting RF current and virtual voltage V_x.

work, and LNA. Our receiver implements these three components at the baseband, and translates their effects to the antenna using the transparency property of passive mixers [18]–[20].

Here we present an expanded description and characterization of the architecture presented in [16], with minor revisions to the implementation to enhance performance (particularly noise). We also confirm some of the theoretical findings in [21] regarding impedance matching and noise performance. Specifically, we confirm in measurement the benefits of 8-phase mixing when implemented in a passive mixer-first receiver architecture. These include a higher impedance matching range, lower noise figure (NF), and rejection of blockers at the harmonics of the LO.

We will show that our passive mixer-first receiver can achieve 1) S_{11} competitive with highly resonant matching networks while tracking the LO frequency, 2) front-end filtering which results in out-of-band linearity competitive with implementations using off-chip high-Q filters, and 3) noise performance close to traditional receiver architectures. Additionally, we will show that we can tune 1) and 2) across a wide range of LO, IF and RF frequencies with digitally programmed baseband circuits.

II. Baseband-Controlled Impedance Matching

A. Analyis of Passive Mixer

In order to analyze the passive mixer, we begin with the model in Fig. 1(a). A quadrature passive mixer is connected directly to an antenna carrying input voltage waveform V_{RF} and with antenna impedance Z_a. Here we model the transistors of the mixer as ideal switches with small series resistance R_{sw}. Each switch is loaded with a capacitor, C_L, and a resistive load R_B. The switches are driven with four 25% duty cycle non-overlapping LO pulses [2], [16], [20], [22]–[24]. The non-overlapping nature of the pulses means that the antenna port will see only one path at a time, so we can treat the four parallel switch resistances as one, as seen in Fig. 1(b) and [25]. As each switch is closed, the signal V_{RF} during that LO pulse is sampled onto the corresponding C_L. The resulting four steady-state voltage levels correspond to differential I and Q down converted baseband signals. The charge on each capacitor slowly leaks through the load R_B to ground. However, as long as R_BC_L is chosen such that its resulting time constant is much larger than a period of the LO, the change in voltage due to this dissipation of charge over a single LO cycle will be small relative to the baseband signals V_I and V_Q.

Because passive mixers are bidirectional, the baseband signals present on the capacitors will also be back up-converted during each LO cycle. As a result, we may define a waveform V_x at the virtual node marked on Fig. 1(b), representing the up-converted and superposed baseband voltages. Furthermore, using this V_x, we can define a current I_{RF} representing the net current coming from the antenna port. Specifically, we expect that I_{RF} will be proportional to both the current discharged through the baseband resistors and the current coming from the antenna. In fact, we can surmise that the effective impedance seen by the antenna will be a series combination of R_{sw} and a scaled version of R_B. The scaling factor for R_B can by calculated by balancing the charge delivered by the input signal to the load C_L [20], [21], [26]:

$$\gamma = \frac{2}{\pi^2}. \tag{1}$$

This implies that if we design the mixer switches to have a small resistance, the impedance presented to the antenna will largely be a function of R_B. We can therefore tune the impedance match with R_B.

B. Effect of Harmonic Conversion

Looking at the waveform V_x in Fig. 1(b), we see that its spectrum must contain the original input signal, V_{RF}. However, the square shape of V_x indicates that it contains signal power at all of the odd harmonics of the LO in addition to the fundamental. The fact that the mixer samples with quadrature LO signals results in image rejection, and so reduces this content by eliminating one image for each harmonic, as seen in Fig. 2 and [27]. The remaining odd harmonics on the antenna port will reradiate,

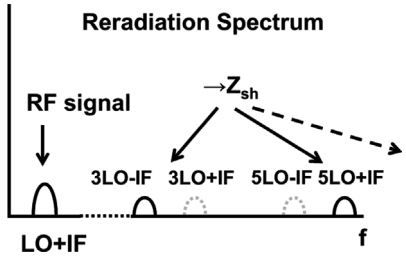

Fig. 2. Spectrum of the reradiation at the antenna interface due to V_x.

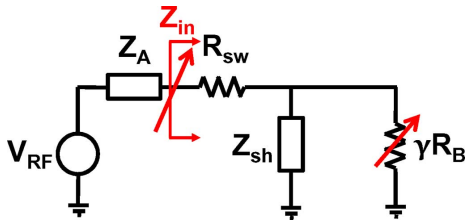

Fig. 3. LTI model for 4-phase passive mixer.

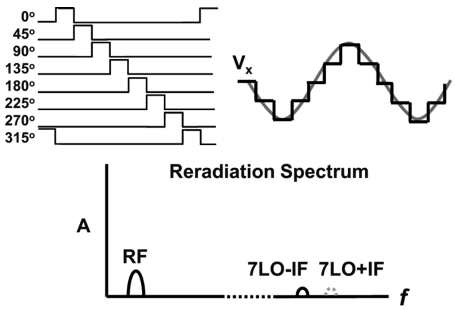

Fig. 4. LO waveforms for an 8-phase passive mixer, approximation of waveform V_x for 8-phase mixer, and resulting reradiation spectrum.

and so dissipate power at these frequencies. Because these harmonics depend on the incoming signal, they represent an additional loss mechanism other than R_B and R_{sw}. Since each harmonic is proportional to, and generated by the received signal on the baseband, this dissipation will reduce the power of the wanted signal. We model this loss as a frequency dependent conductance at each odd harmonic, shunting the mixer output.

$$Y_{a,n} = \frac{1}{n^2}\frac{1}{Z_a(n\omega_{LO}) + R_{sw}}. \tag{2}$$

We calculate the total loss due to harmonic reradiation by summing the effect of each conductance. We model this overall loss as an impedance in shunt with the mixer output, Z_{sh}, defined as [21]

$$Z_{sh} = \left[\sum_{n=3,5,7\ldots}^{\infty} |Y_{a,n}| \exp\left(j\left(\angle Y_{a,n} + \frac{n\pi}{2}\right)\right)\right]^{-1}. \tag{3}$$

For a system with an antenna impedance which is constant across all frequencies, we can perform the sum in (3) and find a value for Z_{sh} as a function of the RF port impedance Z_a and switch resistance R_{sw}:

$$Z_{sh} = \frac{4\gamma}{1-4\gamma}(R_{sw} + Z_a) \approx 4.3(R_{sw} + Z_a). \tag{4}$$

In a typical system, where $R_{sw} = 20\ \Omega$ and $Z_a = 50\ \Omega$, this translates to $Z_{sh} = 300\ \Omega$.

With all the losses now taken into account, we can construct a linear time-invariant (LTI) model for the passive mixer. We have already combined the four switch resistances into one, since only one switch is on at a time. Now we can also do the same for the baseband load R_B, noting that we must multiply it by the scaling factor γ from (1). We must also add the virtual impedance Z_{sh} in shunt with R_B. The resulting model is shown in Fig. 3. This is similar to that presented in [25] but with the inclusion of Z_{sh}. From this model we can write a simple equation for the input impedance of the mixer:

$$Z_{\text{in}} = R_{sw} + \gamma R_B \parallel Z_{sh}. \tag{5}$$

Note that this analysis applies to receive signals with a non-zero IF when R_B from (5) is changed to $Z_B(\omega_{IF})$ to account for reactive components in the baseband (such as C_L) [21].

C. Benefits of 8-Phase Mixing

The expression for Z_{in} from (5) has two components which are a function of the duty cycle of the sampling waveform: γ and Z_{sh}. We can see that Z_{sh} will always limit the influence of R_B on the impedance match. From Section II-B we see that Z_{sh} represents shunting due to power near the harmonics of the LO. In order to reduce harmonic reradiation, we introduce an 8-phase mixer, which contains eight switches instead of four and is driven with eight 12.5% duty cycle LO pulses as seen in Fig. 4 [16], [28]–[30]. The resulting V_x waveform contains power at half as many harmonics as in the 4-phase mixer case (see Fig. 4). Specifically, the 8-phase passive mixer eliminates content at the 3rd, 5th, 11th, 13th harmonics and so on. As a result, Z_{sh}, and the range of Z_{in}, increase dramatically. Additionally, the 8-phase mixer yields a new value for the γ scaling term:

$$\gamma_{8ph} = \frac{2}{\pi^2}(2-\sqrt{2}). \tag{6}$$

For the case of a constant antenna impedance, this implies

$$Z_{sh8ph} = \frac{8\gamma_{8ph}}{1-8\gamma_{8ph}}(R_{sw} + Z_a) \approx 18.9(R_{sw} + Z_a). \tag{7}$$

In a typical system, where $R_{sw} = 20\ \Omega$ and $Z_a = 50\ \Omega$, this translates to $Z_{sh} = 1323\ \Omega$, which is about five times larger than in the 4-phase case.

III. Implementation

Following the analysis in Section II, we have designed a passive mixer-first receiver with tunable baseband impedance matching and the option of using either 4- or 8-phase mixers. Fig. 5 shows the implemented single-chip receiver architecture, including a programmable 4- or 8-phase frequency divider, quadrature passive mixers, baseband LNAs, and harmonic recombination amplifiers.

The receiver was fabricated in 65 nm 1P9M CMOS. The photograph of the chip can be seen in Fig. 6. The total area is 2.5 mm^2, with an active area of 0.75 mm^2. The chip was packaged in a PQFP package and mounted onto a PCB for all

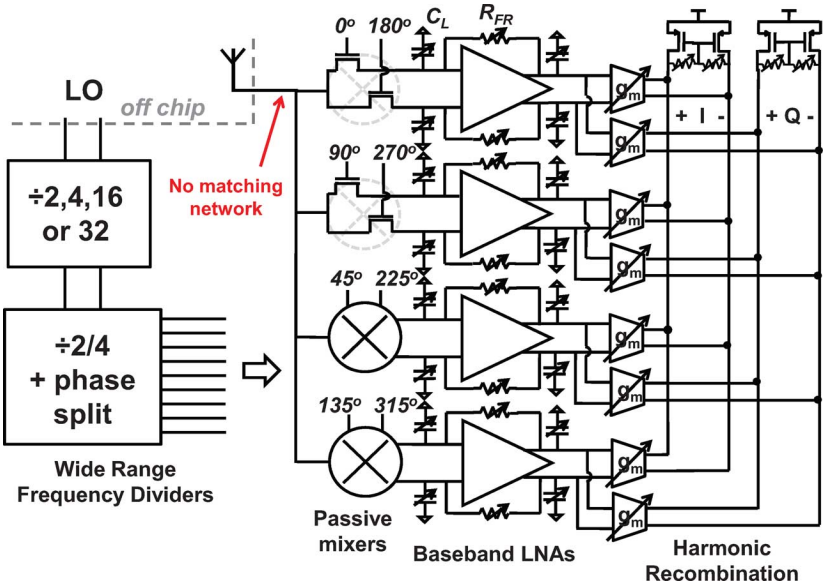

Fig. 5. Block diagram of receiver including frequency dividers, passive mixers, baseband LNAs, and recombination buffers.

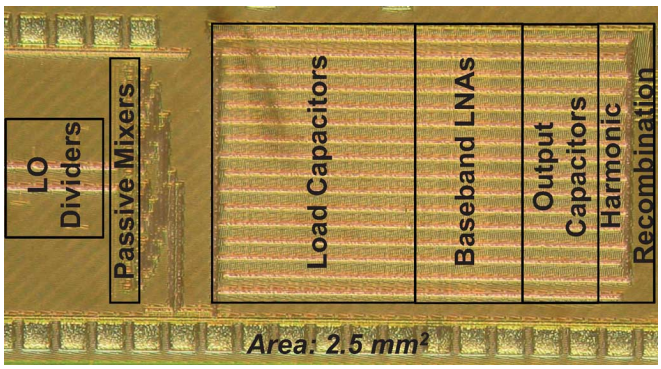

Fig. 6. Picture of receiver implemented in 65 nm CMOS showing functional blocks.

measurements. The circuits operate off dual voltage supplies, with the LO buffer, frequency dividers, and mixers using 1.2 V and the baseband circuitry using 2.5 V. When all the strips are turned on, the 1.2 V supply consumes between 6 and 33 mA, depending on the LO frequency, and the 2.5 V supply consumes 12 mA. This translates to a power consumption of between 37 and 70 mW.

A. Passive Mixer

The passive mixer was implemented with triple-well 1.2 V nMOS transistors with $W = 16\ \mu$m, $L = 60$ nm. The bulk of the mixer devices (and all 1.2 V devices) is tied to the middle of the 2.5 V rail. This allows both the inputs and the outputs of the mixer to sit at levels which bias the baseband amplifiers.

When operating in the 4-phase LO case, there is a maximum of eight of these transistors driven by each LO pulse (eight switches in parallel), which reduces the overall switch resistance. In 8-phase operation, a maximum of four unit switches are driven by each individual pulse. As a result, the effective R_{sw} for 8-phase operation is twice that of the 4-phase case. The receiver offers the option of turning off redundant switches, LO generation circuitry, and baseband circuitry in order to operate in a lower power state with as little as only one transistor for each LO pulse.

B. Frequency Dividers

In order to generate 25% duty cycle quadrature LO pulses, we employed a frequency divide-by-two, composed of two differential latches clocked by opposite phases of the input LO. The standard architecture then combines the outputs of the divider in AND gates to generate quadrature LO pulses [20]. In simulation we found that this approach tended to degrade noise figure, due to flicker noise in the dividers. This effect can be explained by coupling of LO onto the RF port, which is then down converted to baseband. Ideally, a 4-phase mixer will only reradiate at multiples of the 4th harmonic of the effective LO. However, jitter of individual pulse edges results in reradiation at the receive frequency as well. These deviations are especially hard to suppress through device sizing, as the transistors in the dividers must drive significant internal loads at high speed as part of multi-transistor stacks.

Instead, we implemented pulse generation as shown in Fig. 7, by ANDing the divider outputs with the input LO to produce non-overlapping LO phases which are independent of timing variation in the counter itself [31]. This approach was expanded to the 8-phase case by building a four stage differential Johnson counter followed by AND gates to generate eight pulses, split by 45°, but 25% duty-cycle. These pulses were then ANDed with the original LO to generate 12.5% pulses whose edges are insensitive to deviations in the counter.

C. Baseband Feedback Amplifiers

A transistor level schematic of the baseband amplifiers is shown in Fig. 8. The amplifier consists of a fully differential pMOS pair with nMOS loads and digitally controlled common mode feedback resistors R_L which provide three gain settings (between 25 and 35 dB). We chose pMOS transistors for the

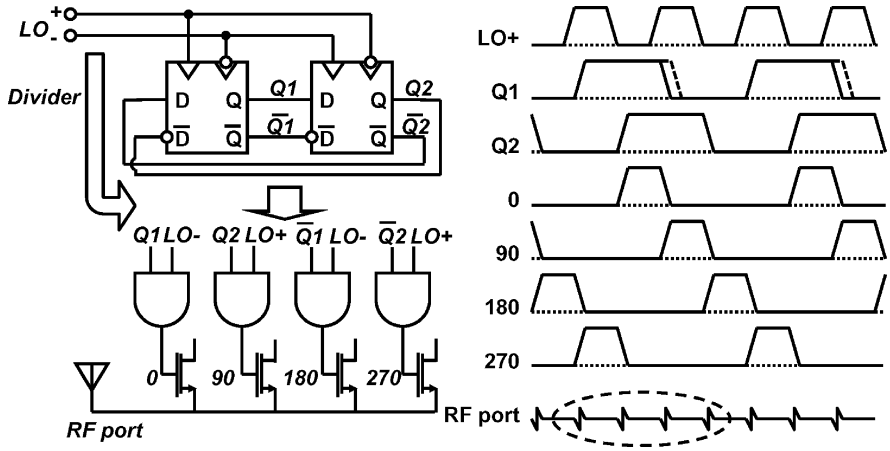

Fig. 7. Schematic and timing diagram of 4-phase frequency divider.

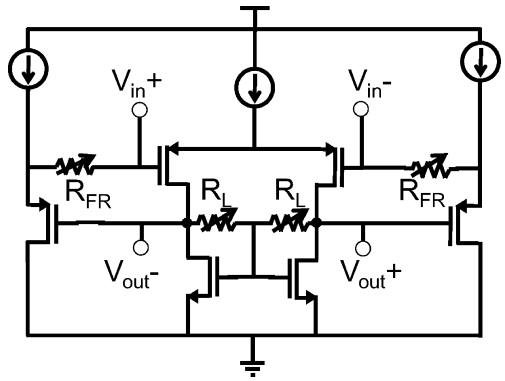

Fig. 8. Transistor-level schematic of baseband LNA.

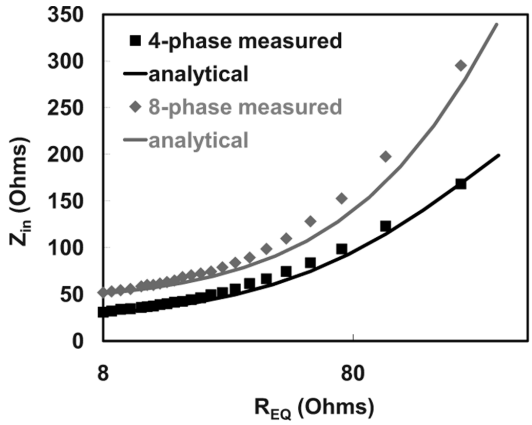

Fig. 9. Comparison of direct measurement of input impedance at $f_{LO} = 100$ MHz with prediction from LTI model for both 4- and 8-phase mixers.

input pair and designed all amplifier transistors with long channels to reduce the $1/f$ corner to below 200 kHz. We implemented the matching resistor R_B from Fig. 1 by wrapping feedback loops around both paths. The feedback consists of a 5-bit tunable resistor R_{FR} connected to the input gates, in series with a source follower to buffer the output.

D. Harmonic Recombination Amplifiers

The receiver has a second stage of amplification (see right of Fig. 5) in which the eight signals are recombined into simple differential I and Q. These consist of tunable-g_m differential pairs which share a common PFET load with common mode feedback and four gain settings (from 16–34 dB in 6 dB steps). When operating in 4-phase mode, the separate but equal I and Q channels (0° and 90°) are simply added together. In 8-phase operation, the 0° phase channel is added with full weight to I, and the 90° phase with full weight to Q. The additional 45° and 135° channels are weighted by $1/\sqrt{2}$ and added to both I and Q, with different polarities. This weighting acts to cancel signals present at half the harmonics of the signal (i.e., the 3rd, 5th, 11th, 13th, etc.) [28]–[30]. The degree of harmonic suppression achievable in these amplifiers is limited by the precision of the $1/\sqrt{2}$ weight (here it was designed to be 11/16) and mismatch in the recombination stage.

In total, the LNAs and the recombination amplifiers provide more than 70 dB of gain with a maximum BW of 20 MHz, limited by the parasitic capacitance of the amplifiers and some fixed capacitance local to the mixer outputs to shunt switching transients.

IV. Impedance Matching: Measurements

To provide a reference for the impedance matching measurements in this section and the following ones, we begin by defining an expected effective impedance, presented to the mixer by the baseband, which incorporates the gain of the feedback amplifier A, the feedback resistor R_{FR} and the scaling factor γ:

$$R_{EQ} = \gamma R_B = \gamma \frac{R_{FR}}{1+A}. \tag{8}$$

In order to confirm the analysis in Section II, we have measured the input impedance of the receiver directly for $f_{LO} = 100$ MHz, $f_{RF} = 101$ MHz. The resulting curves (shown in Fig. 9) show the effect of sweeping the real feedback resistor R_{FR} (scaled to R_{EQ} for both 4-phase and 8-phase operation). We have also included the curves which result from applying (5) for simulated A (30 dB) and independently measured R_{sw} and Z_{sh} (4-phase: $R_{sw} = 20\ \Omega$, $Z_{sh} = 350\ \Omega$; 8-phase: $R_{sw} = 40\,\Omega$, $Z_{sh} = 1100\,\Omega$). As predicted, the effective R_{sw} is about doubled for the 8-phase case. Note also that Z_{sh} is lower than predicted earlier for the 8-phase case. This is because the

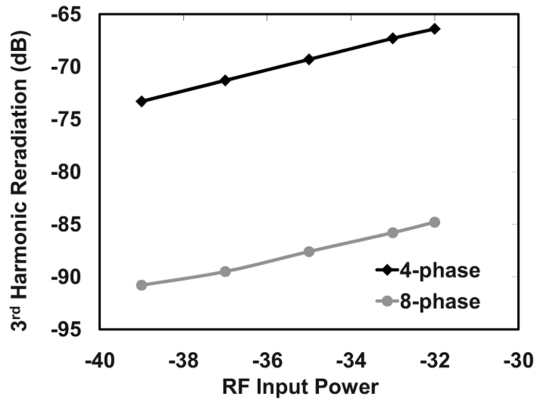

Fig. 10. Measurement of reradiation out of the RF port at 2.999 GHz for an RF signal injected at 1.001 GHz.

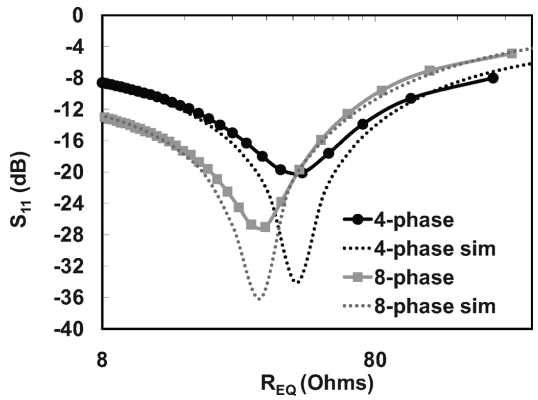

Fig. 11. Comparison of simulation and measurement of S_{11} at $f_{LO} = 1$ GHz vs effective R_B for both 4- and 8-phase mixers.

RF port impedance is frequency dependent. Since higher harmonics account for more of the value of Z_{sh} for the 8-phase case, if the impedance is lower at those higher frequencies, the constant Z_a model will start to fail.

We also measured the harmonic reradiation out of the RF port predicted in Section II, and the difference in reradiation as a result of 8-phase mixing from Fig. 4. In particular, we looked at reradiation of injected RF signal up converted to a higher harmonic (as distinct from simple reradiation of LO signals coupling onto the RF port through mixer switch parasitics). Recall that this harmonic reradiation is the underlying mechanism behind the virtual lossy element Z_{sh} in the LTI mixer model in Fig. 3. Fig. 10 shows the measurement for an RF signal injected at 1.001 GHz with a 1 GHz effective LO, which generates a signal at 2.999 GHz, 1 MHz below the 3rd harmonic of the LO. This harmonic reradiation is indeed proportional to the input RF signal strength, and is reduced by about 18 dB with 8-phase mixing. We also measured direct LO reradiation at 1 GHz to be about -65 dBm. Beyond simply measuring the input impedance, we have also characterized the ability of the receiver to improve an impedance match by tuning R_{FR}. Fig. 11 shows a measurement of S_{11} at $f_{RF} = 1.001$ GHz and $f_{LO} = 1$ GHz as the feedback resistors are swept for both a 4-phase and 8-phase mixer and driven by a 50 Ω source. These curves show that tuning the resistor does in fact allow for a minimum S_{11}.

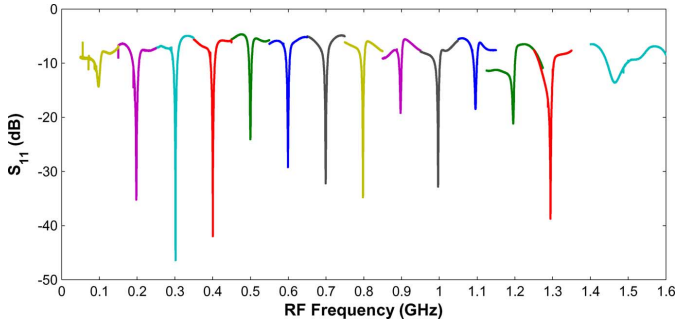

Fig. 12. Measurement of S_{11} around LO frequency stepped by 100 MHz, without any retuning of impedance match.

We have also overlayed simulation results for the same sweeps. In simulation, we modeled the packaging parasitics with a 2 nH series inductance and 300 fF shunt capacitance. These parasitics create a complex antenna impedance which is frequency dependent, and affects Z_{sh}. The minimum is for a different effective R_{EQ} in the different mixing cases, because of their different R_{sw} and Z_{sh} values. However, the match also changes for different IF frequencies, and is assymetric due to the complex antenna impedance (as will be discussed in Section VI-A). The effects of complex antenna impedance on matching are explored further in [21]. Fig. 12 shows that our impedance match is not dependent on the LO frequency to first order but only on the IF (as explained in Section VI-A). Here we tuned the feedback resistor to provide a good match for an LO of 800 MHz. We then moved the LO in 100 MHz steps both upwards and downwards and measured the S_{11} for 100 MHz around the LO using a network analyzer (without retuning baseband components). The impedance match begins to break down at higher frequencies because the package parasitics begin to dramatically impact Z_{sh} at these frequencies.

V. Noise Performance

A. Analysis

In order to evaluate the noise performance of the receiver, we first need to look at the various sources of noise in the circuit shown in Fig. 1(b). There are three fundamental sources of noise: the baseband resistance R_B, the switch resistance R_{sw}, and the thermal noise from the antenna itself, Z_a. Recent work has shown that flicker noise from the switches in passive mixers is negligible [20]. Evaluating the noise figure (inside the baseband bandwidth) from this circuit yields a result which is dominated by R_B, and will always be greater than 3 dB. However, our receiver implements R_B as a feedback resistor wrapped around the baseband low noise amplifier (see Fig. 13). This technique suppresses the noise from R_B by a factor proportional to the gain of the amplifier.

There is an additional source of noise in the circuit: the noise which is down-converted by the mixer at odd harmonics of the LO. We can represent this as a noise current which passes through the RF port at each of the harmonics with

$$\frac{\overline{i_{n,a}^2(n\omega_{LO})}}{Hz} = \frac{4kT}{n^2(Z_a(n\omega_{LO}) + R_{sw})}. \quad (9)$$

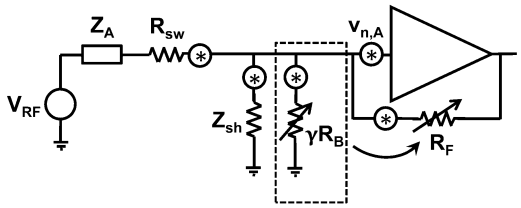

Fig. 13. Schematic displaying noise sources in equivalent receiver model.

However, we note that the sum of the RF port noise currents at the harmonics of the LO is exactly the noise that would be generated by Z_{sh} if it was a real resistor defined by (4). We can therefore use the model in Fig. 13 to find the noise factor of our receiver:

$$F = 1 + \frac{R_{sw}}{R_a} + \frac{Z_{sh}}{R_a}\left(\frac{R_a + R_{sw}}{Z_{sh}}\right)^2 + \gamma\frac{R_{FR}}{R_a}\left(\frac{R_a + R_{sw}}{\gamma R_{FR}}\right)^2 + \gamma\frac{\overline{v_{n,A}^2}}{4kTR_a}\left(\frac{R_a + R_{sw}}{\gamma R_{FR}} + \frac{R_a + R_{sw} + Z_{sh}}{Z_{sh}}\right)^2. \quad (10)$$

The second term represents the noise contributed by R_{sw}. The third term represents the noise contributed by the virtual shunt resistor Z_{sh}. The fourth term represents the noise contributed by the feedback resistor R_{FR}. The fifth term represents the noise contributed by the amplifier. Note that (10) applies to both 4- and 8-phase mixing, with the parameters Z_{sh}, γ, and in our implementation, R_{sw} changing. In the ideal case where R_a is constant across frequency, the 8-phase mixer will have a significantly lower NF than the 4-phase mixer. The analysis leading up to (10) is provided in greater detail in [21].

B. Measurements

Fig. 14 shows the measured DSB NF for the receiver across the frequency range of operation, with an IF at 1 MHz in each case. The frequency range in the 8-phase mode is lower because it divides the input LO by four instead of two as in the 4-phase case. As predicted, the NF for 8-phase operation is lower than for 4-phase operation. NF degradation at higher frequencies is likely due to shunting by package and device parasitics. Such parasitics will also have more effect at higher harmonics, and so will decrease Z_{sh}, degrading NF. In addition, at higher frequencies, the LO pulses driving the mixers are likely to become less ideal, potentially increasing the effective R_{sw} and decreasing Z_{sh}.

Following the analytical result in the previous section, we have also measured the noise figure of the 8-phase receiver for a range of values of R_{FR} (shown in Fig. 15). As predicted from (10), as long as the ratio of R_{FR} to R_a and the ratio of Z_{sh} to R_a are large, the noise figure will be fairly constant, low, and dominated by the baseband amplifier noise. As R_{FR} decreases, these ratios increase and the 3rd and 4th terms in (10) eventually blow up, increasing the noise figure. Fig. 15 also shows the gain of the receiver for the same values of R_{FR}, where gain decreases as R_{FR} (and so R_{EQ}) decreases. Note that while this NF result

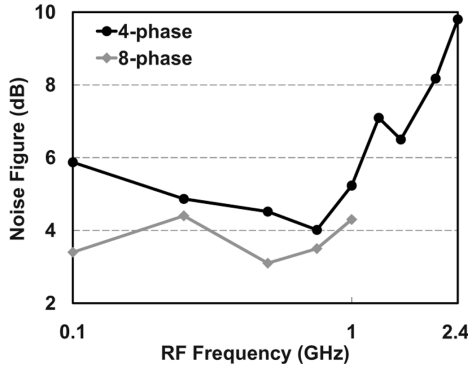

Fig. 14. Measurement of NF vs RF frequency for both 4-phase and 8-phase operation.

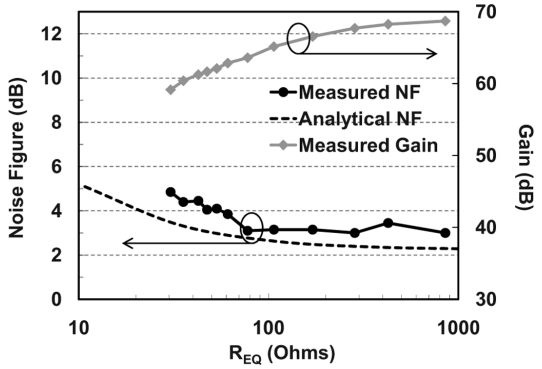

Fig. 15. Measurement of NF and voltage gain vs R_{EQ} as R_{FR} is swept for the 8-phase receiver at $f_{RF} = 900$ MHz, with analytical NF result for comparison.

reaches levels as low as 3 dB, this is still 1–2 dB higher than that predicted in simulations in [21], and by (10), whose result is overlayed with the measurement above. The flicker noise corner of the receiver was also measured and found to be less than 200 kHz under minimum NF conditions.

VI. Blocker Filtering and Linearity

A. Effect of Sampling Capacitor C_L

The presence of the baseband capacitor C_L has several notable effects on the tunable impedance presented to the RF port. As f_{IF} passes the *RC* bandwidth of the baseband, Z_{in} becomes dominated by C_L, and ultimately approaches R_{sw}. By making this capacitor tunable (as shown in Fig. 5), we create a tunable-Q BPF. This transfer of filtering through a switching mixer was first introduced as N-path filtering many years ago [32], and has been used recently in literature to provide filtering for systems which place an LNA at the RF-front-end [18], [26], [33], [34].

In our implemented receiver, we have made C_L digitally controllable with 6 bits of resolution (from 5 pF to 120 pF). Fig. 16 shows measurements of the magnitude of the impedance presented by the receiver for three different values of C_L as RF frequency is swept around a 100 MHz LO. For frequencies very near the LO, the receiver presents the impedance we expect based on the chosen feedback resistance, and as the RF moves away, this impedance is controlled by the capacitor and reduces as $|f_{LO} - f_{RF}|$ increases (or as C_L increases). Note also that

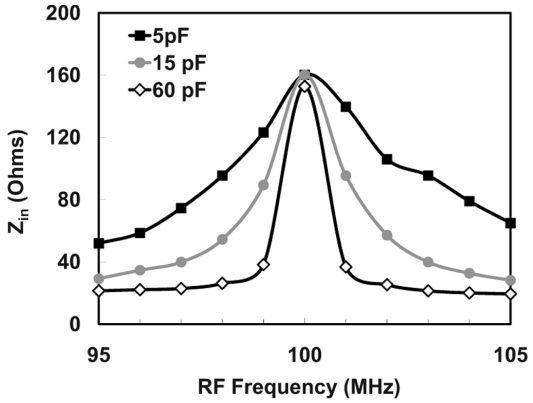

Fig. 16. Direct measurement of tunable bandpass filter created by C_L.

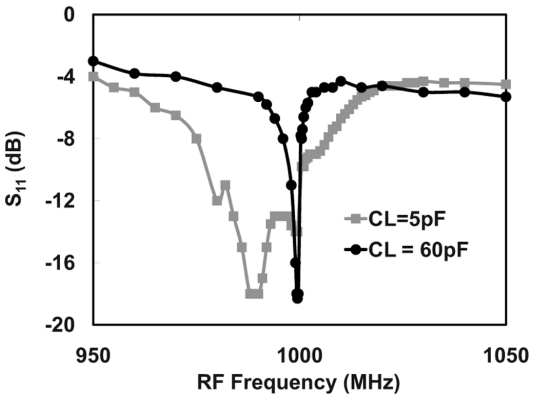

Fig. 17. Measurement of effect on S_{11} curve of tunable bandpass filter created by C_L.

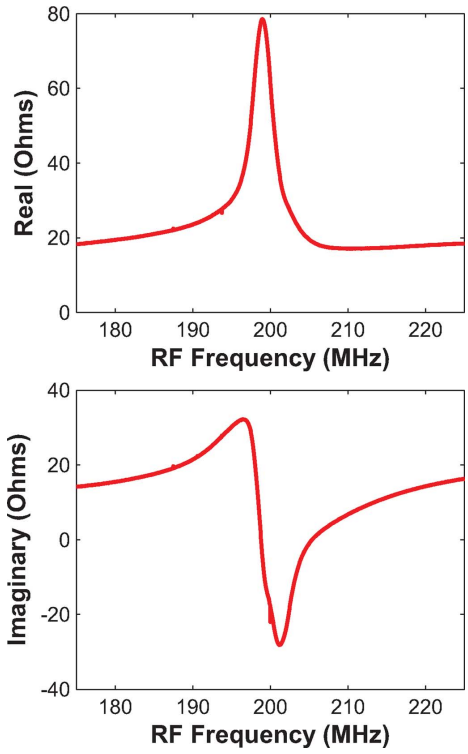

Fig. 18. Measurement of real and imaginary components of impedance presented to the RF port by the receiver.

this impedance reaches a lower limit set by the on resistance of the mixer switches (about 20 Ω).

Furthermore, in Fig. 17, we have confirmed this effect at higher frequency with a measurement of S_{11} for an R_{FR} value tuned to a good match. As we increase the capacitor value, the curve becomes much narrower and the deepest S_{11} notch is closer to the LO.

Finally, we also took direct measurement of both the real and complex components of the input impedance for $f_{LO} = 200$ MHz and $C_L = 60$ pF using a network analyzer (see Fig. 18). The range of a good impedance match here is quite small, as the capacitor dominates the impedance for larger offset frequencies. Additionally, the imaginary component of the impedance demonstrates the interesting property of switching polarities for negative offset frequencies, as predicted theoretically in [21] and [25], and discussed in greater detail in Section IV.

B. IIP2, IIP3, and Out-of-Band Compression Measurements

One implication of having this tunable BPF on the RF port is that it will have a large influence on the out-of-band linearity performance of the receiver [23], [25], [35]. We have characterized the linearity of the receiver for various offset frequencies and capacitor settings. Fig. 19(a) shows out-of-band compression due to a blocker at 1.16 GHz for a 1.2006 GHz RF, for three different C_L values. We define the out-of-band compression level as the power of the blocker which makes the wanted signal diminish by 3 dB. In Fig. 19(b) we have also performed sweeps of the blocker frequency around the 1.2 GHz RF for the three capacitor settings and measured out-of-band compression for each of them. We find that the measured compression levels are well fit by a simple equation [solid lines in Fig. 19(b)]:

$$P_{OB3\text{dB}} = -20\log\left(k1 + \frac{k2}{f_{IFint}^2}\right). \tag{11}$$

where $k1$ and $k2$ are fitting parameters and the form of the equation is consistent with a combination of two mechanisms: 1) a constant outband compression point of $+10$ dBm for far out-of-band blockers which probably reflects compression in the mixer itself, and 2) a frequency dependent term that dominates at lower interferer IF frequencies and follows a $1/f_{IFint}^2$ dependency. This second component becomes weaker with larger capacitor values, and is consistent with a compressive third-order nonlinearity that acts after one pole of blocker filtering, and reflects nonlinearity in the baseband LNAs.

Fig. 19(c) shows the IIP3 measured using two tones (one at 1.22 GHz and the other at 1.2406 GHz), with a 1.2 GHz LO (generating an IM3 product at 1.1994 GHz, which was down-converted to a 600 kHz IF), for two different settings of C_L. We achieve an IIP3 of 27 dBm when a large C_L is chosen, and much worse IIP3 of -8 dBm for the lower C_L. Fig. 19(d) shows the measured IIP3 for various offset frequencies (where the x axis represents the frequency of the tone which is closer to the RF) for both $C_L = 5$ pF and $C_L = 120$ pF. This also shows that with a higher C_L engaged, the receiver maintains good linearity for much closer interferers. As before, this result is well fit by equations of a form similar to (11) which incorporate a combination

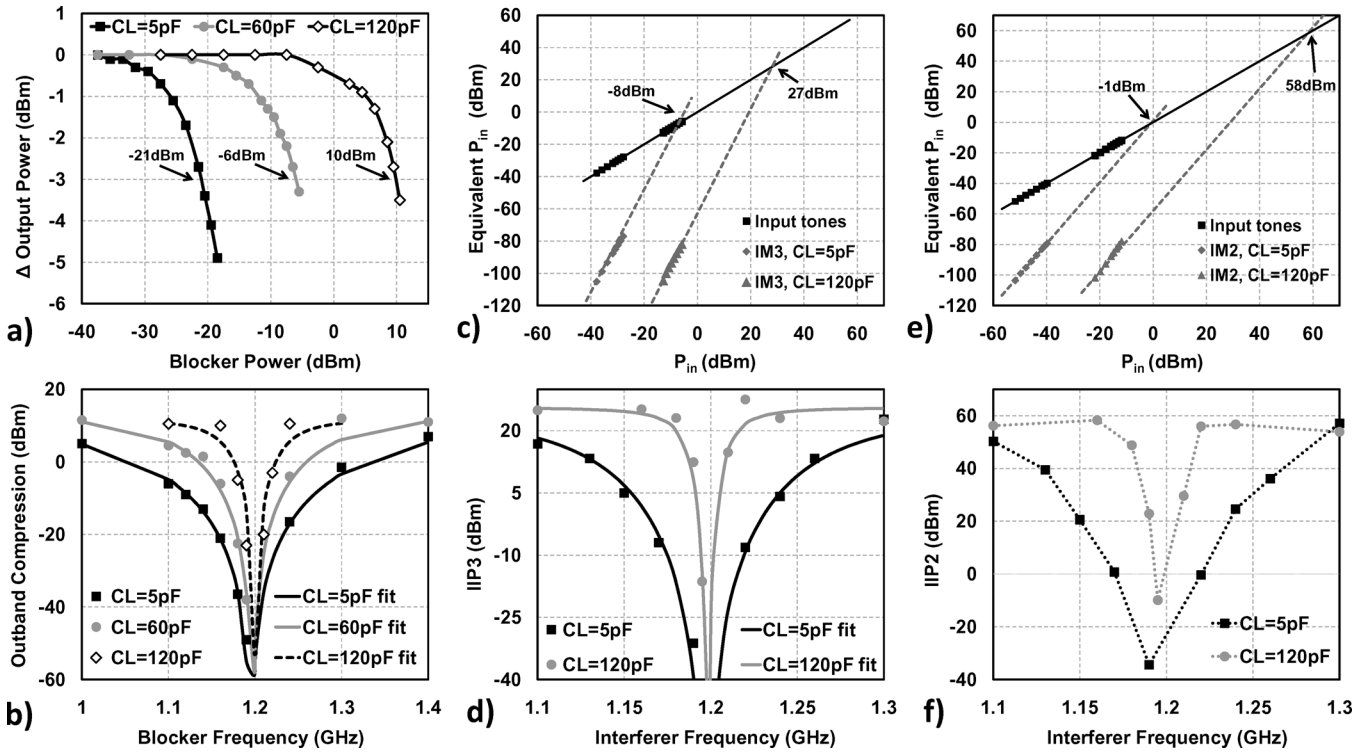

Fig. 19. Measurements of outband compression, IIP3 and IIP2 around $f_{LO} = 1.2$ GHz.

of two mechanisms: a constant, very high IIP3 mechanism (presumably from the mixer), and a frequency dependent component that goes as $1/f^3_{IFint}$ and reflects a third-order nonlinearity in the baseband. These results are consistent with simulations of the baseband amplifiers alone, with the attenuation of the passive mixers and the RC pole accounted for. The out-of-band results are more difficult to replicate in simulation, as discussed in [25]. However, by applying a square-law model to the mixer switches, we computed an out-of-band IIP3 of 24 dBm, which is close to our measurement.

Fig. 19(e) shows the IIP2 for a 2nd order inter-modulation product for two tones (one at 1.22 GHz and one at 1.2206 GHz), for a 1.2 GHz LO, generating an IM2 at 1.2006 GHz. We achieve an IIP2 of 58 dBm when a large C_L is chosen, and much worse IIP2 of -1 dBm for minimum capacitor settings, as 20 MHz is close to being within the bandwidth of the receiver. Fig. 19(f) shows the measured IIP2 for various offset frequencies for both $C_L = 5$ pF and $C_L = 120$ pF. As with other nonlinear effects, as interferers move in-band, they generate larger distortion products. Engaging a larger C_L decreases bandwidth, improving robustness to interferers much closer in frequency. Unlike the third-order nonlinearity described above, IIP2 does not follow a simple-to-fit rule, indicating that the mechanisms generating IIP2 are likely to be more complex than those generating IIP3.

Because the front-end bandwidth of this receiver is programmable, it is possible to trade off bandwidth for interference tolerance. Thus, the receiver can be programmed to receive signals with bandwidths >10 MHz, but can also be reprogrammed to receive narrower bandwidth signals in the presence of blockers that would badly degrade the system if it were set to its original bandwidth.

Because this work focused on demonstrating low noise, impedance tunability and out-of-band linearity performance, little effort was made to linearize the baseband LNAs and recombination amplifiers for in-band linearity. We nonetheless have measured the in-band linearity of the receiver. For a 1 GHz LO, we injected signals at 1.0012 GHz and 1.0016 GHz. These produced an IM2 product at 1.0004 GHz and an IM3 product at 1.0008 GHz. This resulted in an in-band IIP2 of -45 dBm and an in-band IIP3 of -67 dBm. In future designs, in-band linearity can easily be improved by designing higher linearity baseband circuits such as those used in [29]. Indeed, a sensible SDR-style approach would be to make linearity (traded off against power consumption) a programmable feature of the baseband.

C. Harmonic Suppression

In addition to characterizing the susceptibility of the receiver to general wideband interferers, we also measured the ability of the 8-phase mixer and recombination amplifiers to reduce the effect of blockers at the harmonics of the LO frequency. Because we have no RF front-end filter, the mixer will downconvert signals present at those harmonics.

We set up the receiver with an input LO of 2 GHz, for an effective LO of 500 MHz. In order to directly compare the 4-phase case with the 8-phase case, an additional divide-by-two is engaged for the 4-phase case such that both will receive signals around 500 MHz. We then measured the difference in gain between signals injected at the fundamental (499 MHz)

and those injected at the 3rd and 5th harmonics (1.499 GHz and 2.499 GHz, respectively). In the 4-phase case, the output power for the 3rd harmonic was 11 dB less than the fundamental, and the 5th harmonic output was 19.9 dB less. This is fairly consistent with the 1/3 and 1/5 weights which accompany these harmonics in the Fourier series of the square wave sampling signals. For the 8-phase case, which actively rejects these harmonics, the output due to the 3rd harmonic was 35.4 dB less than the fundamental and that due to the 5th harmonic was 42.6 dB less.

The harmonic rejection ratio achieved here is not sufficient to eliminate the influence of large blockers at the harmonics of the LO, limiting its applicability to some wireless standards. The limitations of our implementation come from the late harmonic recombination, coming after a first stage with 30 dB of gain. However, recent works have presented harmonic rejection schemes which provide 60–80 dB of rejection (depending on implementation) [29], [36]. These techniques could easily be applied to our design as well, providing a similar degree of rejection.

VII. Complex Feedback

A. Motivation

While radios are most often designed to match a constant, purely real antenna impedance of 50 Ω, in reality, the actual impedance of an antenna can vary widely at different operating frequencies and in different environments. Additionally, the mere presence of parasitics on the PCB, package, bond wires and pads inherently make the effective antenna impedance complex. As seen in Fig. 11, the center of the S_{11} notch for our passive mixer-first receiver is not directly centered around the LO but offset by several megahertz. This is due to the baseband complex impedance presented by the capacitor C_L interacting with the parasitic complex components of the antenna port.

Fig. 18, which shows the impedance presented by the receiver as a function of IF frequency, shows that the imaginary component of $Z_{\rm in}$ looks negative for positive IF and positive for negative IF. On the upper sideband of the LO, the antenna port sees the impedance presented by the baseband port as a function of the IF, but the lower sideband sees the *complex conjugate* of this impedance [21], [25]. This implies that the required complex conjugate match for a complex antenna impedance can only exist at a single IF frequency.

In principle, the imaginary component of this match is tunable since we have control over the value of the capacitor. However, using the sampling capacitor to provide a complex impedance match has the disadvantage that it will limit the bandwidth of a good match. Worse, it can only be used to match one polarity of imaginary antenna impedance, or in other words it can only match that impedance on one of the side bands of the LO.

B. Implementation

In order to solve the problem of matching to complex antenna impedances, we have implemented the circuit in Fig. 20, which modifies our original feedback amplifiers to provide "complex feedback". Here we connect feedback resistors from the output of the I-channel of the amplifier to the input of the Q-channel,

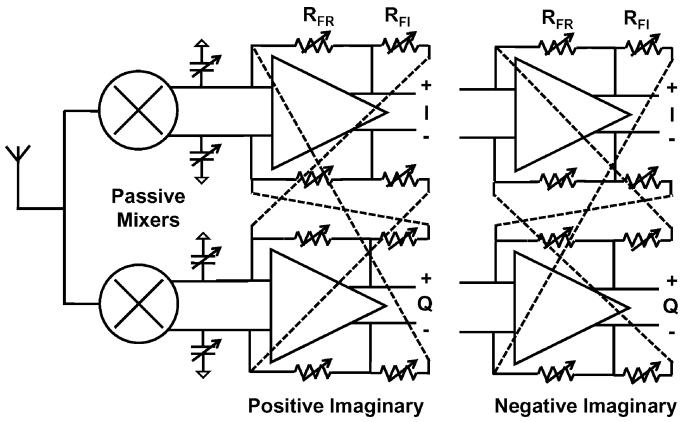

Fig. 20. Receiver schematic with complex feedback.

and vice versa. These additional feedback paths present a 90° phase shifted (and scaled by R_{FI}) version of the original signals back to the amplifier inputs. This phase translates to a complex impedance presented to the antenna port through the passive mixer. A similar feedback technique is utilized in [37] and [38] but was used to modify the phase of a filter rather than to present a complex impedance to the input. Implementing R_{FI} in the same way as R_{FR}, and allowing for its polarity to be switched (as in Fig. 20) provides a programmable complex impedance match.

Analysis of the circuit in Fig. 20 yields an expression for the new baseband impedance Z_B where the real part is still mostly a function of the real feedback resistor R_{FR}, and the imaginary component depends on the value of the resistor R_{FI}. Note that R_{EQ} from (8) will change with the new Z_B from (12) to become Z_{EQ}.

$$Z_B = \left[\left(\frac{1+A}{R_{FR}} + \frac{1}{R_{FI}}\right) \pm j\frac{A}{R_{FI}}\right]^{-1}. \qquad (12)$$

One additional note is that because of the relative phases of sine and cosine, we actually need to flip the polarity of the feedback resistors from the Q channel to the I channel, in order to get the same equivalent phase shift. Of course this effect only operates within the bandwidth set by the baseband capacitors.

C. Measurements

In order to measure the effects of complex feedback, we set up the receiver to receive an RF frequency around 500 MHz and swept the RF frequency using a network analyzer (see 27 Ω curve in Fig. 21). We tuned the impedance match with the real feedback resistor to provide a deep S_{11} notch, without yet engaging the complex feedback (see 36 Ω curve). We then turned on the complex feedback path with a positive R_{FI} value and swept the RF frequency again, as expected this shifted the IF frequency of the optimum S_{11} (see 36||+j72Ω curve). We repeated this measurement with the opposite polarity of complex feedback, which results in a notch on the opposite side of the LO frequency.

To show that complex feedback can be used to provide matching on both sidebands in the face of significant impedance mismatch on the RF port, we moved the effective LO frequency

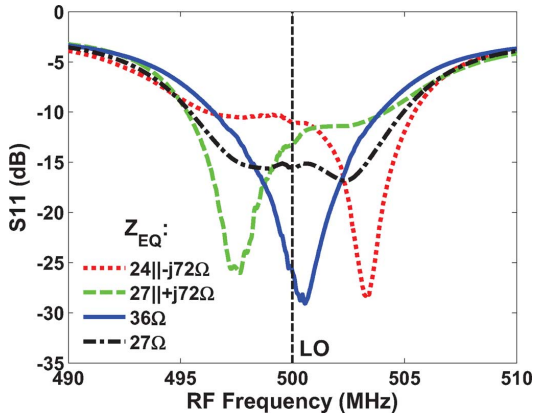

Fig. 21. Measurement of moving S_{11} curve for both polarities of complex feedback, compared to curves without any complex feedback, with both tuned and untuned R_{FR}.

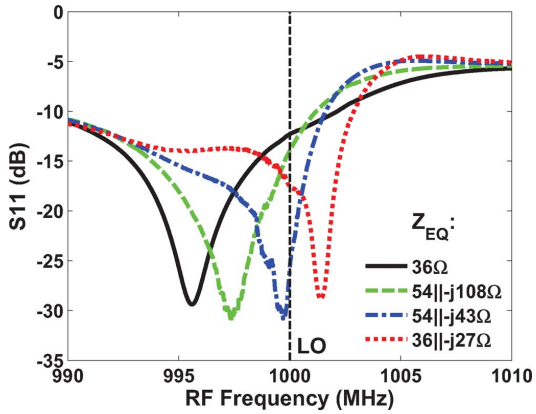

Fig. 22. Measurement showing complex feedback pushing notch of S_{11} curve to the other sideband of the LO.

to 1 GHz, where capacitive parasitics were much more dominant. Fig. 22 shows that without complex feedback, S_{11} is minimum at a significant IF offset from the LO. Engaging complex feedback shifts this optimum to very close to the LO frequency, and by further decreasing R_{FI} (effectively increasing the influence of complex feedback), we can move the S_{11} notch to the other sideband of the LO, dramatically improving S_{11} for that sideband.

The potential for instability is a limitation of complex feedback. As the magnitude of the cross-channel conductance is increased (R_{FI} is decreased), the inputs of the amplifier can see enough phase rotation to elicit oscillation in the baseband amplifiers (the baseband essentially becomes a ring oscillator). This can be an issue if the imaginary matching term is significantly stronger than the real term, and represents a limit on the complex antenna impedance that can be matched reliably.

Finally, we measured the effect of complex feedback on the NF of the receiver. Fig. 23 shows the DSB NF of the 8-phase mode receiver for swept R_{FI} of both polarities for an LO at 900 MHz and a 1 MHz IF. Not surprisingly, one polarity provides a better NF than the other because it provides an improved complex conjugate impedance match to the RF port.

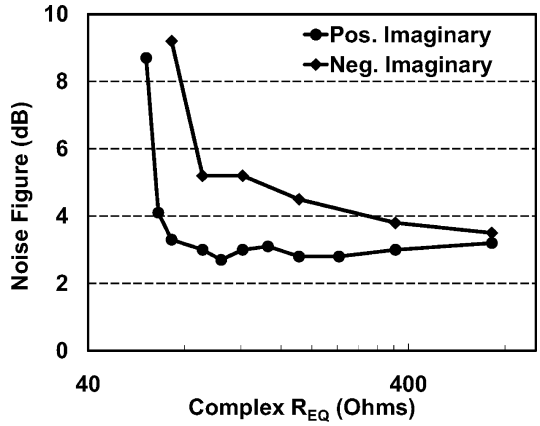

Fig. 23. Measurement of NF of receiver vs imaginary component of Z_{EQ} for swept complex feedback resistor R_{FI}, in both polarities of complex feedback.

TABLE I
SUMMARY OF PERFORMANCE

Technology	65nm
Frequency Range	0.1-2.4GHz
Gain	40-70dB
DSB NF	4dB±1dB
Out-of-band IIP3	+25dBm
Out-of-band IIP2	+56dBm
Power	37-70mW
Power Supply	1.2V (RF) / 2.5V (Baseband)
Impedance Match	$Z_{EQ} = (8-250) \parallel \pm j(8-250)\Omega$

VIII. CONCLUSION

We have presented a software-defined radio receiver capable of NF close to 3 dB, out of band IIP3 up to 27 dBm and 0.1–2.4 GHz frequency tuning range, as summarized in Table I. The architecture uses a passive mixer-first, LNA-less approach in order provide digital control of parameters in the entire antenna interface. The transparency of passive mixers translates the impedance on one side of them to the other. We used this effect to translate a LPF on the baseband to a BPF on the RF port, allowing for the rejection of out-of-band interferers. Feedback resistors on baseband differential LNAs allow for a tunable real impedance match within the bandwidth of the BPF. Additionally, we demonstrate "complex feedback", which creates an effective complex impedance on the RF port by using feedback between the in-phase and quadrature paths of the baseband. We use this complex impedance to match complex RF port impedances. We show that the S_{11} notch tracks the LO frequency of the receiver, and is to first order only a function of the circuits present on the baseband. Finally, the receiver achieves competitive noise performance with state of the art receivers. This work demonstrates a receiver architecture that for the first time provides programmable RF impedance matching and filtering without sacrificing performance.

REFERENCES

[1] M. Kitsunezuka, S. Hori, and T. Maeda, "A widely-tunable, reconfigurable CMOS analog baseband IC for software-defined radio," *IEEE J. Solid-State Circuits*, vol. 44, no. 9, pp. 2496–2502, Sep. 2009.

[2] M. Soer, E. Klumperink, Z. Ru, F. E. van Vliet, and B. Nauta, "A 0.2-to-2.0 GHz 65 nm CMOS receiver without LNA achieving 11 dBm IIP3 and 6.5 dB NF," in *IEEE ISSCC Dig. Tech. Papers*, Feb. 2009, vol. 52, pp. 222–223.

[3] R. van de Beek, J. Bergerboet, H. Kundur, D. Leenaerts, and G. van de Weide, "A 0.6-to-10 GHz receiver front-end in 45 nm CMOS," in *IEEE ISSCC Dig. Tech. Papers*, Feb. 2008, vol. 51, pp. 128–129.

[4] R. Bagheri, A. Mirzaei, S. Chehrazi, M. E. Heidari, M. Lee, M. Mikhemar, W. Tang, and A. A. Abidi, "An 800-MHz–6-GHz software-defined wireless receiver in 90-nm CMOS," *IEEE J. Solid-State Circuits*, vol. 41, no. 12, pp. 2860–2876, Dec. 2006.

[5] A. van Bezooijen, M. A. de Jongh, C. Chanlo, L. Ruijs, F. van Straten, R. Mahmoudi, and A. H. M. van Roermund, "A GSM/EDGE/WCDMA adaptive series-LC matching network using RF-MEMS switches," *IEEE J. Solid-State Circuits*, vol. 43, no. 10, pp. 2259–2268, Oct. 2008.

[6] H. Song, B. Bakkaloglu, and J. T. Aberle, "A CMOS adaptive antenna-impedance-tuning IC operating in the 850 MHz-to-2 GHz band," in *IEEE ISSCC Dig. Tech. Papers*, Feb. 2009, vol. 52, pp. 384–385.

[7] J. Liu, G. Vandersteen, J. Craninckx, M. Libois, M. Wouters, F. Petre, and A. Barel, "A novel and low-cost analog front-end mismatch calibration scheme for MIMO-OFDM WLANs," in *Proc. IEEE Radio and Wireless Symp.*, Jan. 2006, pp. 219–222.

[8] J. Ryynanen, S. Lindfors, K. Stadius, and K. Halonen, "Integrated circuits for multi-band multi-mode receivers," *IEEE Circuits Syst. Mag.*, vol. 6, pp. 5–16, Jun. 2006.

[9] K. Lim, S.-H. Lee, S. Min, S. Ock, M.-W. Hwang, C.-H. Lee, K.-L. Kim, and S. Han, "A fully integrated direct-conversion receiver for CDMA and GPS applications," *IEEE J. Solid-State Circuits*, vol. 41, no. 11, pp. 2408–2416, Nov. 2006.

[10] J. Craninckx, M. Liu, D. Hauspie, V. Giannini, T. Kim, J. Lee, M. Libois, D. Debaillie, C. Soens, M. Ingels, A. Baschirotto, J. Van Driessche, L. Van der Perre, and P. Vanbekbergen, "Fully reconfigurable software-defined radio transceiver in 0.13 μm CMOS," in *IEEE ISSCC Dig. Tech. Papers*, Feb. 2007, pp. 346–347.

[11] A. Bourdoux, J. Craninckx, A. Dejonghe, and L. Van der Perre, "Receiver architectures for software-defined radios in mobile terminals: the path to cognitive radios," in *Proc. IEEE Radio and Wireless Symp.*, Jan. 2007, pp. 535–538.

[12] T. Tikka, J. Ryynanen, and K. Halonen, "Multiband receiver for base-station applications," in *Proc. IEEE Radio and Wireless Symp.*, Jan. 2008, pp. 871–874.

[13] J. A. M. Jarvinen, J. Kaukovuori, J. Ryynanen, J. Jussila, K. Kivekas, M. Honkanen, and K. A. I. Halonen, "2.4-GHz receiver for sensor applications," *IEEE J. Solid-State Circuits*, vol. 40, no. 7, pp. 1426–1433, Jul. 2005.

[14] D. G. Tucker, "The history of the homodyne and synchrodyne," *J. British Inst. Radio Eng.*, vol. 14, no. 4, pp. 143–154, Apr. 1954.

[15] B. Cook, A. Berny, A. Molnar, S. Lanzisera, and K. Pister, "Low power 2.4 GHz transceiver with passive RX front-end and 400 mV supply," *IEEE J. Solid-State Circuits*, vol. 41, no. 12, pp. 2757–2766, Dec. 2006.

[16] C. Andrews and A. C. Molnar, "A passive-mixer-first receiver with baseband-controlled RF impedance matching <6 dB NF, and <27 dBm wideband IIP3," in *IEEE ISSCC Dig. Tech. Papers*, Feb. 2010, pp. 46–47.

[17] S. Zhou and M.-C. Chang, "A CMOS passive mixer with low flicker noise for low-power direct-conversion receiver," *IEEE J. Solid-State Circuits*, vol. 40, no. 5, pp. 1084–1093, May 2005.

[18] N. Kim, L. Larson, and V. Aparin, "A highly linear SAW-less CMOS receiver using a mixer with embedded Tx filtering for CDMA," *IEEE J. Solid-State Circuits*, vol. 44, no. 8, pp. 2126–2137, Aug. 2009.

[19] A. Mirzaei, H. Darabi, J. C. Leete, X. Chen, K. Juan, and A. Yazdi, "Analysis and optimization of current-driven passive mixers in narrowband direct-conversion receivers," *IEEE J. Solid-State Circuits*, vol. 44, no. 10, pp. 2678–2688, Oct. 2009.

[20] A. Mirzaei, H. Darabi, J. C. Leete, and Y. Chang, "Analysis and optimization of direct-conversion receivers with 25% duty-cycle current-driven passive mixers," *IEEE Trans. Circuits Syst. I, Reg. Papers*, vol. 57, no. 9, pp. 2353–2366, Sep. 2010.

[21] C. Andrews and A. C. Molnar, "Implications of passive mixer transparency for impedance matching and noise figure in passive mixer-first receivers," *IEEE Trans. Circuits Syst. I, Reg. Papers*, vol. 57, no. 12, Dec. 2010, DOI: 10.1109/TCSI.2010.2052513.

[22] M. Camus, B. Butaye, L. Garcia, M. Sie, B. Pellat, and T. Parra, "A 5.4 mW/0.07 mm^2 2.4 GHz front-end receiver in 90 nm CMOS for IEEE 802.15.4 WPAN standard," *IEEE J. Solid-State Circuits*, vol. 43, no. 8, pp. 1372–1383, Aug. 2008.

[23] H. Khatri, L. Liu, T. Chang, P. Gudem, and L. Larson, "A SAW-less CDMA receiver front-end with single-ended LNA and single-balanced mixer with 25% duty-cycle LO in 65 nm CMOS," in *IEEE Radio Frequency Integrated Circuits Symp. Dig.*, Jun. 2009, pp. 13–16.

[24] D. Kaczman, M. Shah, M. Alam, M. Rachedine, D. Cashen, L. Han, and A. Raghavan, "A single-chip 10-band WCDMA/HSDPA 4-Band GSM/EDGE SAW-less CMOS receiver with DigRF 3G interface and $+90$ dBm IIP2," *IEEE J. Solid-State Circuits*, vol. 44, no. 3, pp. 718–739, Mar. 2009.

[25] H. Khatri, P. S. Gudem, and L. E. Larson, "Distortion in current commutating passive CMOS downconversion mixers," *IEEE Trans. Microwave Theory Tech.*, vol. 57, no. 11, pp. 2671–2681, Nov. 2009.

[26] A. Ghaffari, E. A. M. Klumperink, and B. Nauta, "A differential 4-path highly linear widely tunable on-chip bandpass filter," in *IEEE Radio Frequency Integrated Circuits Symp. Dig.*, Jun. 2010, pp. 299–302.

[27] M. C. M. Soer, E. A. M. Klumperink, P.-T. de Boer, F. E. van Vliet, and B. Nauta, "Unified frequency-domain analysis of switched-series-*RC* passive mixers and samplers," *IEEE Trans. Circuits Syst. I, Reg. Papers*, vol. 57, no. 10, pp. 2618–2631, Oct. 2010.

[28] A. Molnar, B. Lu, S. Lanzisera, B. W. Cook, and K. S. J. Pister, "An ultra-low power 900 MHz RF transceiver for wireless sensor networks," in *Proc. IEEE Custom Integrated Circuits Conf.*, Oct. 2004, pp. 401–404.

[29] Z. Ru, N. Moseley, E. A. M. Klumperink, and B. Nauta, "Digitally enhanced software-defined radio receiver robust to out-of-band interference," *IEEE J. Solid-State Circuits*, vol. 44, no. 12, pp. 3359–3375, Dec. 2009.

[30] J. A. Weldon, R. S. Narayanaswami, J. C. Rudell, L. Lin, M. Otsuka, S. Dedieu, L. Tee, K.-C. Tsai, C.-W. Lee, and P. Gray, "A 1.75-GHz highly integrated narrowband CMOS transmitter with harmonic-rejection mixers," *IEEE J. Solid-State Circuits*, vol. 36, no. 12, pp. 2003–2015, Dec. 2001.

[31] X. He and J. van Sinderen, "A low-power, low-EVM, SAW-less WCDMA transmitter using direct quadrature voltage modulation," *IEEE J. Solid-State Circuits*, vol. 44, no. 12, pp. 3448–3458, Dec. 2009.

[32] L. Franks and F. Witt, "Solid-state sampled-data bandpass filters," in *IEEE ISSCC Dig. Tech. Papers*, Feb. 1960, pp. 70–71.

[33] H. Darabi, "A blocker filtering technique for SAW-less wireless receivers," *IEEE J. Solid-State Circuits*, vol. 42, no. 12, pp. 2766–2773, Dec. 2007.

[34] A. Mirzaei, X. Chen, A. Yazdi, J. Chiu, J. Leete, and H. Darabi, "A frequency translation technique for SAW-less 3G receivers," in *IEEE Symp. VLSI Circuits*, Jun. 2009, pp. 280–281.

[35] N. Kim, V. Aparin, and L. E. Larson, "A resistively degenerated wideband passive mixer with low noise figure and high IIP2," *IEEE Trans. Microwave Theory Tech.*, vol. 58, no. 4, pp. 820–830, Apr. 2010.

[36] E. A. Keehr and A. Hajimiri, "A rail-to-rail input receiver employing successive regeneration and adaptive cancellation of intermodulation products," in *IEEE Radio Frequency Integrated Circuits Symp. Dig.*, Jun. 2010, pp. 47–50.

[37] O. E. Erdogan, R. Gupta, D. G. Yee, J. C. Rudell, J.-S. Ko, R. Brockenbrough, S.-O. Lee, E. Lei, J. L. Tham, H. Wu, C. Conroy, and B. Kim, "A single-chip quad-band GSM/GPRS transceiver in 0.18 μm standard CMOS," in *IEEE ISSCC Dig. Tech. Papers*, Feb. 2005, vol. 48, pp. 318–319.

[38] K.-W. Cheng, K. Natarajan, and D. Allstot, "A current reuse quadrature GPS receiver in 0.13 μm CMOS," *IEEE J. Solid-State Circuits*, vol. 45, no. 3, pp. 510–523, Mar. 2010.

Caroline Andrews (S'09) received the B.S. degree in electrical engineering from the University of Virginia, Charlottesville, in 2008. She is currently working towards the Ph.D. degree in electrical engineering at Cornell University, Ithaca, NY.

Her research focuses on developing highly tunable front-ends for software-defined radios.

Alyosha C. Molnar (S'03–M'07) received the B.S. degree in engineering with highest honors from Swarthmore College, Swarthmore, PA, in 1997, and the M.S. and Ph.D. degrees in electrical engineering from the University of California, Berkeley, in 2003 and 2007, respectively.

From 1998 to 2002, he was with the RF IC Group at Conexant Systems, Inc. (now Skyworks Solutions, Inc.), Newport Beach, CA, where he developed their first generation GSM direct conversion receiver. In August 2007 he joined the faculty of the School of Electrical and Computer Engineering, Cornell University, Ithaca, NY.